Iraqi Journal of Physics, 2023 *Vol. 21 No. 3, PP. 64-76*
https://doi.org/10.30723/ijp.v21i3.1133 *P-ISSN: 2070-4003*
E-ISSN: 2664-5548

Influence of NiTi Spring Dimensions and Temperature on the Actuator Properties

Zina A. Al Shadidi*[1a], Ahmad Kadhum Falih[2b], Mahdi Hasan Suhail[1c], Soha Salem Hiadrah[3d]
[1]*Department of Radiology, Al Mamoon University Collage, Baghdad, Iraq*
[2]*Department of Radiology, Collage of Medical Techniques, Al Farahidi University, Baghdad, Iraq*
[3]*Department of Physics, Collage of Education, University of Abyan, Abyan, Yemen*
[b]Email: algebori64@gmail.com, [c]Email: mahdi.h.suhail@almamonuc.edu.iq
[d]Email: khula.phy.edu@aden-univ.net
[a*]Corresponding author: zabaqer@yahoo.com

Abstract

Nitinol (NiTi) is used in many medical applications, including hard tissue replacements, because of its suitable characteristics, including a close elastic modulus to that of bones. Due to the great importance of the mechanical properties of this material in tissue replacements, this work aims to study the hysteresis response in an attempt to explore the ability of the material to remember its previous mechanical state in addition to its ability to withstand stress and to obtain the optimal dimensions and specifications of the manufacturer of NiTi actuators. Stress-strain examination is done in a computational way using a mutable Lagoudas MATLAB code for various coil radii, environment temperatures, and coil lengths. The computational methodology was done by varying the dimensions and the ambient temperature for the simulated NiTi spring actuator. The hysteresis loop is studied by increasing the external stress for a reversible martensitic transformation. The coil radius, spring height, and wire radius affect the spring force and deformations. In the same way, these parameters affect the strain and stress point values. These changes are shown through the martensite and austenite start and finish values. The NiTi hysteresis loop narrows with increasing ambient temperature or initial spring height. At a higher temperature, the force supplied to the actuator must be less for the same deformation; therefore, a higher ambient temperature provides more efficiency for the shape memory devices and a longer lifetime for the actuator.

Article Info.

Keywords:
Super elasticity, Nitinol, Actuator, MATLAB, Hysteresis loop.

Article history:
Received: May. 26,2023
Revised: Aug. 16, 2023
Accepted: Aug. 18, 2023
Published: Sep. 01,2023

1. Introduction

Nitinol, nickel titanium equiatomic alloy (NiTi), is a unique material that exhibits the shape memory effect and superelasticity [1-12]. These properties make the NiTi material valuable for various industries, such as biomedical devices, aerospace engineering, and robotics [13]. One of the critical characteristics of Nitinol is its hysteresis loop, which is a graphical representation of the material's response to changes in temperature and stress. Nitinol has two phases: austenite and martensite, which have completely different crystal structures. It undergoes a reversible transformation between the two phases. Nitinol undergoes phase transformation, leading to changes in shape and mechanical properties. The hysteresis process is a unique behavior that happens in materials through the loading and unloading path differences. Understanding the hysteresis loop of Nitinol is critical in designing and developing devices. In this regard, researchers are continually exploring new ways to leverage Nitinol's behavior to create innovative and efficient products.

There are many applications based on the elasticity of shape-memory alloys where large recoverable deformations are required. Most applications based on superelasticity are in biomedical applications [14-29].

Shape-memory alloys (SMAs) can be used as actuators. Actuators are used as

Iraqi Journal of Physics by IJP is licensed under a Creative Commons Attribution 4.0 International License.

thermal switch-control coolants in automobiles, as a flap control for controlling airflow in air conditioners, as air dampers for multi-function electric ovens, and as a thermal mixing valve in faucets. Also, they are used in various aerospace applications and microrobots [30-35]. Actuators work with a large force generated by a constrained shape memory alloy with element recovery. It utilizes the shape memory effect to generate force and motion.

Developments in the thermo-mechanical constitutive modeling of shape memory alloys were done by Boyd and Lagoudas (1996) [36] and motivated by Dimitris et al. (2012) [37]. Their model improved the smooth transition between the thermal and mechanical responses, resulting in a computationally efficient and accurate analysis tool within a thermodynamically consistent mathematical framework. They introduced a model that captures the behavior of SMAs under three-dimensional thermo-mechanical loading paths with good accuracy. Waldemar et al. (2013) [38] found that the conducted tests showed that the SMA wire is a strongly non-linear and hysteretic object, and the use of resistance as feedback in positioning systems built based on thin SMA wires is better than temperature feedback.

The thermo-mechanical behavior of pseudoelastic shape memory alloy helical springs was also discussed by Soren et al. (2016) [39] through a constitutive description of the shape memory alloy based on the framework developed by Lagoudas and co-workers, incorporating two modifications related to hardening and sub-loop functions. The spring model takes into account both bending and torsion of the spring wire, thus representing geometrical nonlinearities. The experiments considered different deflection amplitudes, frequencies, and ambient temperatures that influence spring behavior. Weirich and Kuhlenkötter (2019) [40] evaluated possible applications for SMAs based on the requirements in the field of aircraft interiors. They gathered requirements regarding industry standards through detailed literature research and user interviews. They found their solutions through a detailed analysis of the requirements and certification standards for electromechanical systems and verified that SMA-based actuation has many possible applications in aircraft interiors. Nevertheless, there are still some critical requirements for SMA, and the above-proposed solutions lay the foundation for further research.

In hysteresis processes, permanent plastic strain remains in the material [41-45]. The additional permanent strain associated with each consecutive cycle gradually decreases until it practically ceases to accumulate further. The hysteresis behavior (hysteresis loops) occurs when the SMA is subjected to a cyclic thermal load. When the SMA transforms from the austenite phase to the martensite phase and the SMA completely changes shape, a small, unrecoverable strain remains. After a large number of cycles, all the accumulated strain recovers its original shape. That means the material does not recover its original shape after thermal expansion and strain; it takes time to return to its original shape. This hysteresis behavior leads to a decrease in the efficiency of the actuator. The actuator lifetime is particularly critical since it limits the usability of shape memory actuators in applications requiring many thousands of activation cycles. Cyclic mechanical loading of the material leads to classical material fatigue due to crack formation and growth, also known as structural fatigue [36].

For all the above reasons, this study sheds light on the stability of the Nitinol shape memory alloy and the factors affecting the Nitinol actuator's performance, represented by the actuator's dimensions and the ambient temperature. The variations in mechanical and thermal properties were investigated by changing the simulated Nitinol spring actuator dimensions and the ambient temperature. The hysteresis loop was studied by increasing the external stress for a reversible martensitic transformation. The

hysteresis loop appears during SMA material training, where training is the process of repeatedly loading and unloading the material until its response becomes consistent.

2. Methodology

In this study, simulations for an actuator of NiTi wire of 50% Ni and 50% Ti (equiatomic) where used. The constitutive description of the shape-memory alloy is based on the framework developed by Boyd and Lagoudas [36]. The NiTi wire makes a helical spring. Any helical spring has dimensioning parameters of initial coil radius r_0, assumed constant, wire radius C, initial height h_0, N number of windings, and finally the wire being assumed to be of constant length [43], where:

$$\mathrm{L} = \sqrt{\mathrm{h_0}^2 + (2\pi \mathrm{N r_0})^2} \qquad (\mathbf{1})$$

The geometrical properties of Nitinol springs are given as follows:

C =0.25 mm, $r_o = 1.25\ mm$, $h_o = 6\ mm$, N= 6

The force of spring is given by [33]:

$$\mathrm{F} = \frac{2\mathrm{C}^3}{3\mathrm{r_0}} \cos\alpha_0 (\pi\tau^* + 2\alpha^* \tan\alpha_0) \qquad (\mathbf{2})$$

where: θ_0 is the initial pitch angle, $\tau^*, \alpha^*$is the shear stress and strain, respectively, while α_0 represents the strain before deformation.

The stress σ is given by [46, 47]:

$$\sigma = \frac{F}{2\pi r_0} \qquad (\mathbf{3})$$

$$\theta_0 = \arctan\left(\frac{h_0}{2\pi N r_0}\right) \qquad (\mathbf{4})$$

and θ is the pitch angle:

$$\theta = \arcsin\left(\frac{\mathrm{u}}{\mathrm{L}} + \sin\theta_0\right) \qquad (\mathbf{5})$$

where u is the spring displacement (deformation) and h is the spring height.

The strain ($\in$) is given by:

$$\in = \frac{\mathrm{u}}{\mathrm{h}} \qquad (\mathbf{6})$$

The superelasticity Lagoudas model reported by Hartl et al. (2010) [48] was adopted to investigate the effect of ambient temperature on the actuator's continuity and the shape of the stress-strain hysteresis loop. In this case, the Lagoudas model is based on macroscopic observations (variables), including spring temperature, stress, and strain. Also, the effect of spring length, spring radius, and wire length on the actuator's performance was studied via the hysteresis loop analysis.

The Lagoudas model determines the actuator's displacement (deformation) due to the effect of applied force; hence, the hysteresis loop is a deformation function of applied force. Stress and strain equations were added to the model to plot the regular

hysteresis loop, which represents strain as a function of stress. The Lagoudas model was used to find the required variables in this research.

3. Results and Discussion

Studying the NiTi actuator, the variations in mechanical and thermal properties were investigated by changing the simulated Nitinol spring dimensions and ambient temperature. The hysteresis loop was studied by increasing the external stress for a reversible martensitic transformation. The hysteresis loop appears during SMA material training, where training is the process of repeatedly loading and unloading the material until its response becomes consistent.

The hysteretic response of the Nitinol material was studied due to the effects of changing the coil radius r_0, keeping the wire radius $C = 0.25$ mm, ambient temperature $T = 25^{o}C$, initial spring height $h_0 = 6$ mm, and number of coils N=6 fixed.

Fig. 1 shows the hysteresis loops of the 50% Ni NiTi-shaped memory alloy for a coil radius of 1.25 mm. There are two types of hysteresis loop curves: the force-deformation hysteresis loop and the stress-strain hysteresis loop. The coil radius affected our simulated equiatomic NiTi actuator, where the coil radius was (1.25 mm, 1.3 mm, 1.35mm, 1.4 mm, and 1.45mm).

Fig. 2 shows the deformation-spring force hysteresis loop. The points of transformation determined by the tangent line, where the transformation starts and ends, primarily increased during the loading cycle (upper plateau) and decreased during the unloading cycle (lower plateau). At the upper plateau, the point of Martensite start (M_s) was of a deformation equal to 6.667 mm and a spring force equal to (6.121 N). These values increased along the upper plateau to become the martensite finish point (M_f) of a deformation equal to (19.19mm) and a spring force equal to 8.089 N. At the lower plateau, the austenite start point ($A_{s)}$ has a deformation of 14.55 mm and spring force of 4.748 N. These values decreased along the lower plateau to become the austenite finish point (A_f), with deformation equal to 3.434 mm and spring force equal to 1.973 N.

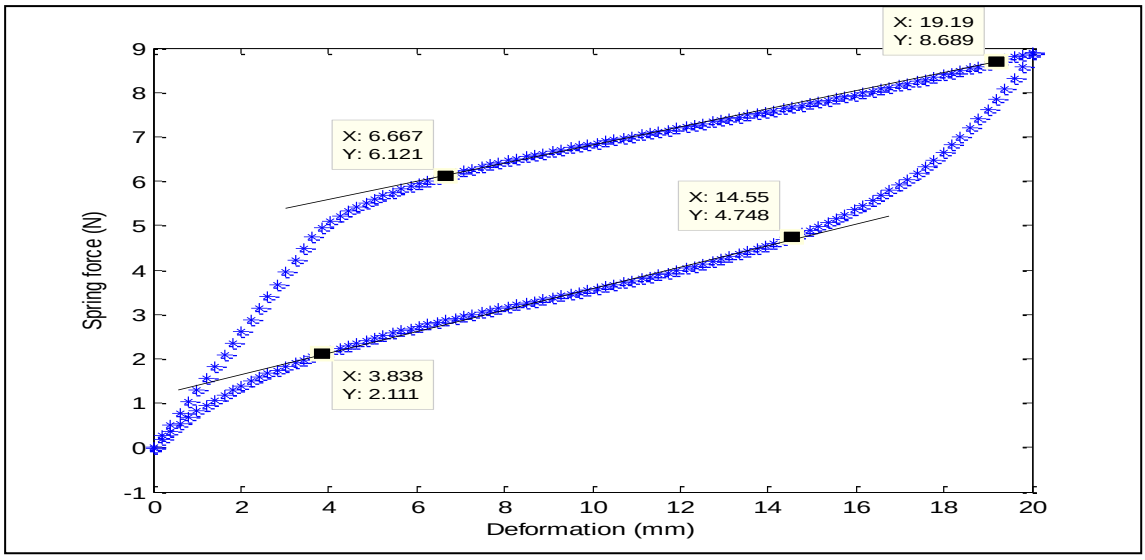

Figure 1: Deformation-spring force hysteresis loop with coil radius $r_0 = 1.25$ mm.

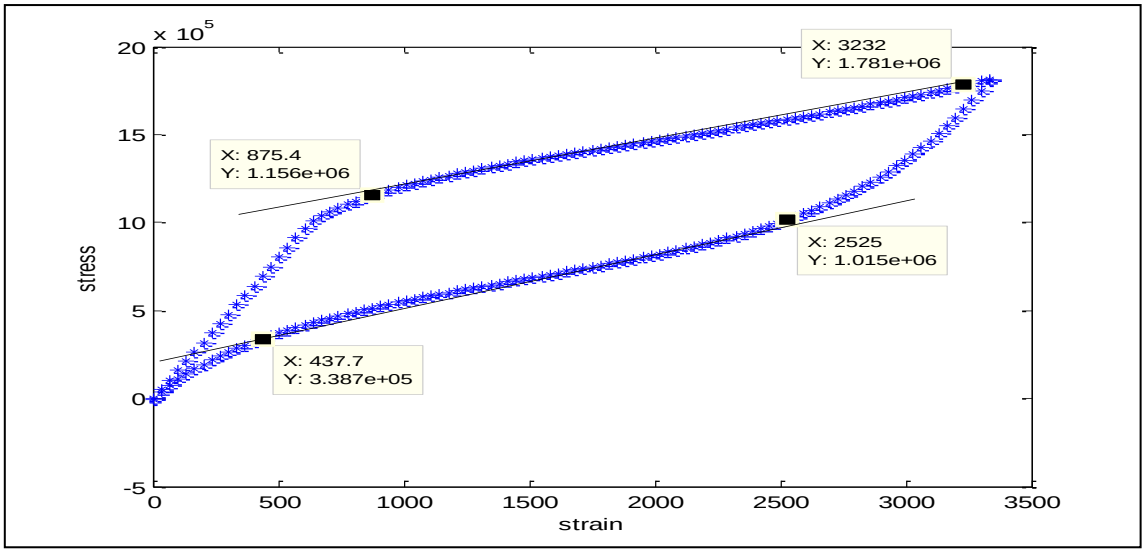

Figure 2: Stress-strain hysteresis loop with coil radius $r_0 = 1.25\ mm$.

For different values of coil radius (1.3, 1.35, 1.4, and 1.45) mm, 20 hysteresis loops were obtained, from which the transformation points (M_s, M_f, A_s, and A_f) values were determined and listed in Tables 1 and 2. The size of the hysteresis loops in these cases was the same, but the points of transformation (M_s, M_f, A_s, and A_f) changed with the increase in coil radius. The same behavior appeared in the stress-strain hysteresis loops. The size of these loops became narrow; this means that the size of the hysteresis loop depends on the coil radius.

Table 1: The effect of coil radius on the deformation and force parameters

$T = 25\ C^{\circ}$, $C = 0.25$ mm, $N = 6$, $h_0 = 6$ mm

Coil radius $r \times 10^{-3}$mm	Deformation(mm)				Spring force (N)			
	M_s	M_f	A_S	A_f	M_s	M_f	A_S	A_f
1.25	6.667	19.19	14.55	3.838	6.121	8.689	4.748	2.111
1.3	6.869	19.39	14.14	3.636	5.798	8.099	4.352	1.904
1.35	7.071	20	13.94	3.434	5.503	7.666	4.071	1.716
1.4	7.273	20	13.74	3.232	5.233	7.174	3.824	1.544
1.45	7.879	20	13.33	3.03	5.067	6.743	3.555	1.385

Table 2: The effect of coil radius on the stress and strain parameters.

$C = 0.25$ mm, $h_0 = 6$ mm, $N = 6$, $T = 25\ C^{\circ}$

Coil radius r (mm)	Strain				Stress (N/m^2)			
	M_s	M_f	A_S	A_f	M_s	M_f	A_s	A_f
1.25	875.4	3232	2525	437.7	1.156×10^6	1.761×10^6	1.015×10^6	3.387×10^5
1.3	1077	3266	2492	538.7	1.072×10^6	1.534×10^6	8.707×10^5	3.33×10^5
1.35	1111	3300	2256	572.4	9.436×10^5	1.332×10^6	6.918×10^5	2.997×10^5
1.4	1145	3333	2222	606.1	8.343×10^5	1.165×10^6	6.046×10^5	2.707×10^5
1.45	1212	3333	2189	572.4	7.477×10^5	1.021×10^6	5.314×10^5	2.282×10^5

where $M_s, and\ M_f$ represents the martensite start and finish values, respectively. While $A_s\ and\ A_f$ represents austenite start and finish values, respectively.

Fig. 3 (A) shows the change in the transformation points with increasing the coil radius. While Fig. 3(B) shows the spring force points decrease with the increase of the coil radius.

20 hysteresis loops of the 50% Ni NiTi shape memory alloy were determined for different spring heights that affected our simulated equiatomic NiTi actuator of (6 mm, 8mm, 10 mm, 12 mm, and 14 mm). The points of transformation are (M_s, M_f, A_s, and A_f) were determined by the tangent line. The behavior of these points is similar to the previous case, where it increased on the high plateau and decreased in the low plateau, as shown in Tables 3 and 4. The size of each loop became smaller as the initial spring height increased.

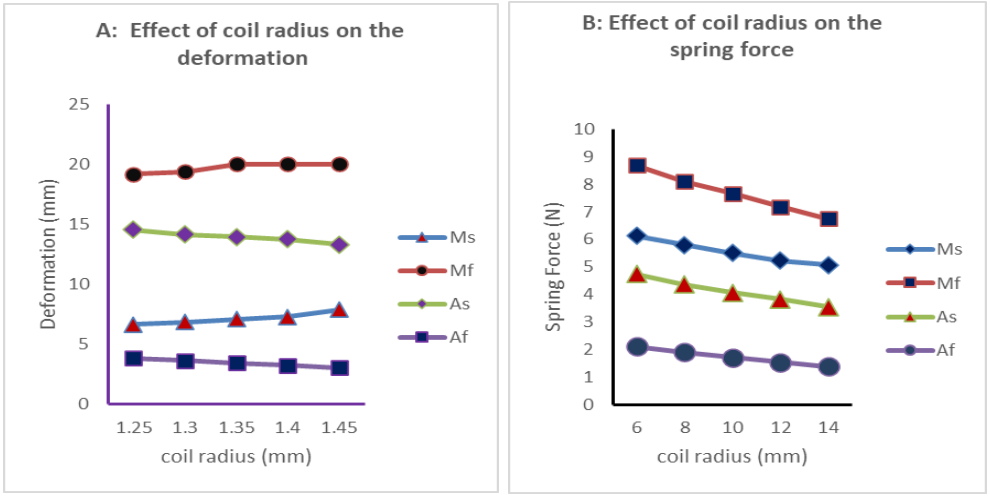

Figure 3: (A) Represents the effect of coil radius on the deformation, (B) Represents the effect of coil radius on the spring force.

Table 3: The effect the initial spring height on the deformation and force parameters.

$T = 25\ C^{\circ}$ $C = 0.25mm$ $N = 6$ $r_0 = 1.25mm$

Springheight h (mm)	Deformation(mm)				Spring force (N)			
	M_s	M_f	A_S	A_f	M_s	M_f	A_s	A_f
6	5.05	18.99	13.74	3.434	5.594	8.637	4.476	1.973
8	5.253	19.19	13.94	3.232	5.673	8.689	4.54	1.9
10	5.455	20	14.55	3.03	5.835	9.573	4.933	1.838
12	5.657	20	14.75	2.828	5.956	9.945	5.116	1.763
14	5.859	20	14.96	2.626	6.076	10.35	5.314	1.662

Table 4: The effect of the initial spring height on the stress and strain parameters.

$C = 0.25\ (mm)$, $r_0 = 1.25\ (mm)$, $N = 6$, $T = 25\ C^{\circ}$

Spring height h (mm)	Strain				Stress (N/m^2)			
	M_S	M_f	A_s	A_f	M_S	M_f	A_s	A_f
6	1044	3030	2256	437.7	1.224×10^6	1.719×10^6	8.992×10^5	3.387×10^5
8	756.6	2424	1768	353.5	1.222×10^6	1.842×10^6	9.558×10^5	3.565×10^5
10	565.7	1939	1394	343.4	1.204×10^6	1.906×10^6	9.59×10^5	4.055×10^5
12	454.5	1633	1145	286.2	1.198×10^6	1.992×10^6	9.622×10^5	4.072×10^5
14	346.3	1414	995.7	245.3	1.152×10^6	2.089×10^6	9.955×10^5	4.088×10^5

Fig. 4(A) shows the spring height effect on the deformation martensite and austenite starts and finish points. While Fig. 4(B) shows the effect of the spring height on the spring force martensite and austenite start and finish points, for the 20 hysteresis loops, deformation points (M_s, M_f, A_s, and A_f) changed with increasing the spring height, while the spring force points(M_s, M_f, A_s, and A_f) decreased.

The austenite points (As and A_f) and martensite points (M_s and M_f) were determined, as the wire radius C was changed between (0.25-0.45) mm, keeping the other variables fixed, as shown in Tables 5 and 6.

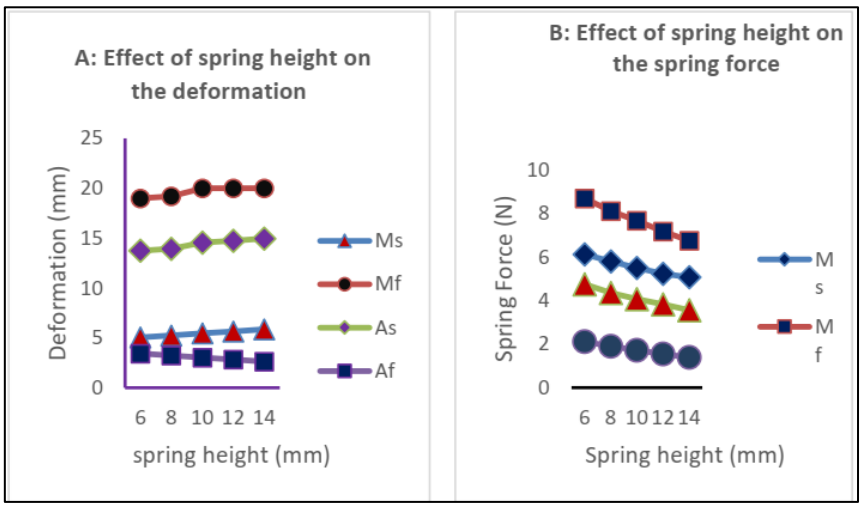

Figure 4: (A) Represents the effect of spring height on the deformation, (B) Represents the effect of spring height on the spring force.

Table 5: The effect of the wire radius on the deformation and force parameters.

$T = 25\,°C$ $h_0 = 6$ (mm) $N = 6$ $r_0 = 1.25$(mm)

Wire radius C (mm)	Deformation(mm)				Spring force (N)			
	M_S	M_f	A_s	A_f	M_S	Ms	A_s	A_f
0.25	5.859	20	13.74	3.636	5.884	15.72	4.476	2.043
0.3	5.o51	18.59	13.74	3.434	10.25	15.72	7.95	3.503
0.35	4.848	17.58	13.54	3.434	16.86	25.85	7.95	5.56
0.4	4.04	16.36	11.72	2.02	24.78	39.62	12.95	5.638
0.45	3.636	14.55	11.52	1.818	35.34	56	27.99	6.631

Table 6: The effect of the wire radius on the stress and strain parameters.

$h_0 = 6$ (mm), $r_0 = 1.25$ (mm), $N = 6$, $T = 25\,°C$

Wire radius (mm)	Strain				Stress (N/m^2)			
	M_S	M_f	A_s	A_f	M_S	M_f	A_s	A_f
0.25	909.1	3333	2424	606.1	1.17×10^6	1.815×10^6	9.672×10^5	4.162×10^5
0.3	875.4	3131	2391	639.7	2.115×10^6	3.225×10^6	1.699×10^6	7.621×10^5
0.35	774.4	2929	2290	538.7	3.39×10^6	5.267×10^6	2.685×10^6	1.092×10^6
0.4	673.4	2694	1987	471.4	5.049×10^6	7.999×10^6	3.746×10^6	1.454×10^6
0.45	572.4	2323	1987	370.4	7.08×10^6	1.11×10^7	5.991×10^6	1.658×10^6

The size of the hysteresis loops remained the same as the wire radius values was changed (0.25 mm, 0.3 mm, and 0.35 mm), but at wire radius values of 0.4 mm, and 0. 45 mm, the loops became narrow. Fig. 5(A) shows that the (M_s, M_f, A_s, and A_f)

deformation points decreased with increasing the wire radius. Fig.5(B) shows that spring force points (M_s, $M_f, A_f,$ and A_f) increased with increasing the wire radius. Our results agree with those of Auricchio et al. [49].

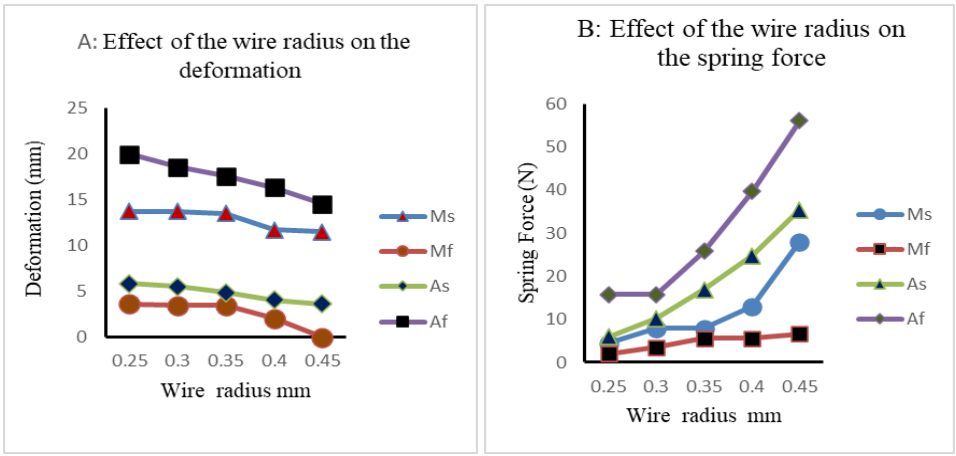

Figure 5: (A) Represents the effect of wire radius on the deformation, (B) Represents the effect of wire radius on the spring force.

The authors focused on examining the dependence of the actuator's characteristics on temperature to observe the decrease in its efficiency due to thermoelastic martensitic transitions that may occur when the stress associated with the forward transformation is totally recovered through the reverse transformation. The results of changing the temperature while keeping the other variables fixed are shown in Tables 7 and 8.

The temperatures used to study its effect on our simulated equiatomic NiTi actuator were (5, 10, 15, 20, 25, 30, 35, 40, 45, 50, and 55) ^{o}C.

Figs. 6 and 7 show the deformation-spring force and stress-strain hysteresis loops at 5^{o}C. The loop was large area and did not form a closed orbit. The same happened at a temperature of 10^{o}C. The loop's behavior was asymptotic at temperatures of 15^{o}C, 20^{o}C, and 25^{o}C; the loops were of a closed form and narrow. As the temperature increased, the hysteresis loops continued to narrow until reaching a temperature of 55^{o}C. The size of the hysteresis loops, due to changes in temperature, increases at low temperatures and becomes narrower at high temperatures. Our results agreed with those of Soren et al. [39] and Toptas et al. [50].

Table 7: The effect of the temperature on the deformation and force parameters.

$\mathbf{C = 0.25(mm),\ \ r_0 = 1.25(mm),\ \ N = 6\ \ \ h_0 = 6\ (mm)}$

Temperature(^{o}C)	**Deformation(mm)**				**Spring force (N)**			
	M_S	M_f	A_s	$\mathbf{A_f}$	$\mathbf{M_S}$	$\mathbf{M_f}$	$\mathbf{A_s}$	$\mathbf{A_f}$
5	2.02	19.8	15.35	3.03	2.406	6.007	2.194	-0.434
10	2.626	20	16.16	3.838	3.137	6.714	3.297	0.333
15	3.03	20	16.36	4.04	3.744	7.488	4.125	0.9957
20	3.262	20	16.57	4.242	4.184	8.2	4.955	1.651
25	4.04	20	16.77	4.444	5.01	8.91	5.788	2.3
30	4.242	20	16.97	4.848	5.53	9.618	6.623	3.003
35	4.646	20	17.17	5.051	6.113	10.32	7.46	3.64
40	5.051	20	17.37	5.657	6.68	11.02	8.301	4.406
45	5.657	20	17.58	5.859	7.499	11.72	9.144	5.036
50	6.061	20	17.78	6.263	8.085	12.41	9.991	5.732
55	6.465	20	17.98	7.071	8.659	13.1	10.68	6.578

Table 8: The effect of the temperature on the stress and strain parameters

$C = 0.25\ (mm),\ r_0 = 1.25\ 6(mm),\ N = 6,\ h = 6(mm)$

Temperature(^{0}C)	Strain				Stress (N/m^2)			
	M_S	M_f	A_s	A_f	M_S	M_f	A_s	A_f
5	370.4	3333	2593	707.1	5.145×10^5	1.235×10^6	4.649×10^5	-4.1×10^4
10	437.7	3333	2626	774.4	6.39×10^5	1.38×10^6	6.3116×10^5	1.062×10^5
15	505.1	3333	2660	875.4	7.627×10^5	1.525×10^6	7.977×10^5	2.623×10^5
20	538.7	3333	2694	909.1	8.524×10^5	1.671×10^6	8.52×10^5	3.996×10^5
25	606.1	3333	2727	942.8	9.683×10^5	1.815×10^6	9..683$\times 10^5$	5.337×10^5
30	673.4	3333	2761	976.4	1.08×10^6	1.959×10^6	1.3×10^6	6.706×10^5
35	841.8	3333	2795	1010	1.31×10^6	2.103×10^6	1.406×10^6	8.043×10^5
40	875.4	3333	2828	1044	1.406×10^6	2.2453×10^6	1.636×10^6	9.366×10^5
45	942.8	3333	2862	1077	1.528×10^6	2.387×10^6	1.805×10^6	1.068×10^6
50	1010	3333	2896	1145	1.647×10^6	2.528×10^6	1.975×10^6	1.211×10^6
55	1077	3333	2929	1212	1.764×10^6	2.666×10^6	2.145×10^6	1.355×10^6

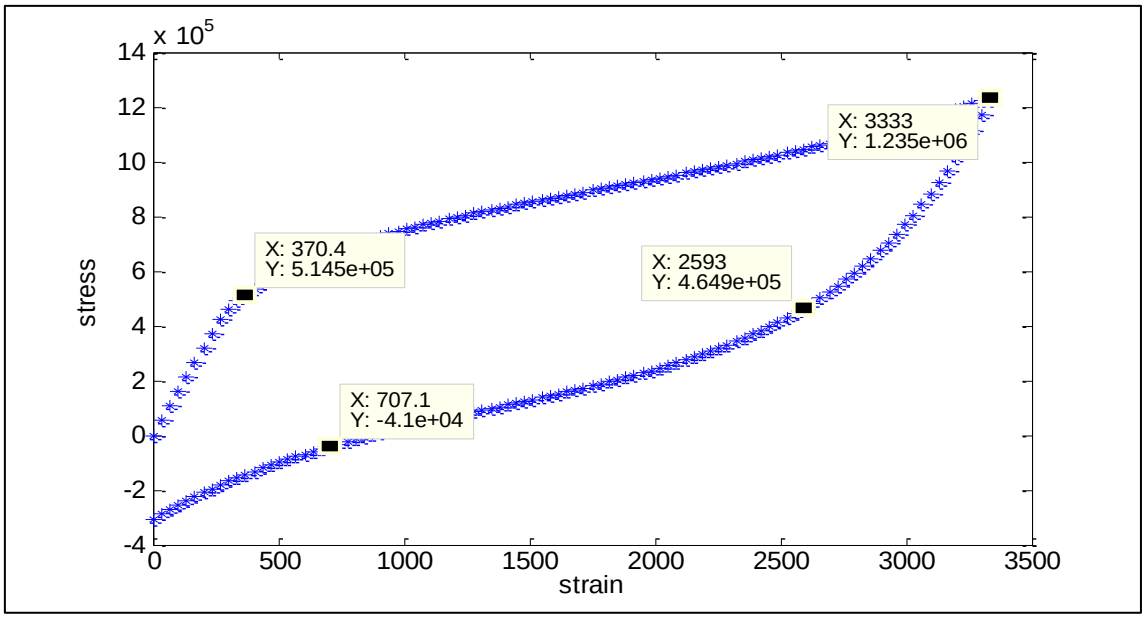

Figure 6: Deformation-spring force hysteresis loop at 5°C.

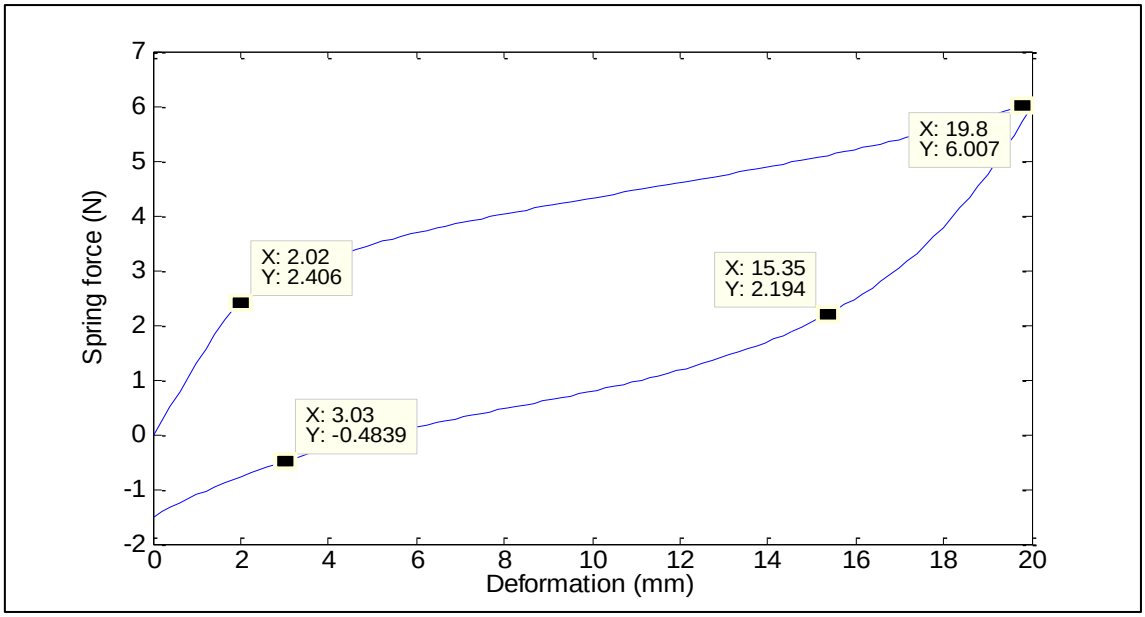

Figure 7: Stress-strain hysteresis loop at 5°C.

For every (force-deformation) hysteresis loop, the points of transformation increased primarily during the loading cycle (upper plateau) and decreased during the unloading cycle (lower plateau). At 5°C: for the upper plateau, the point transformation M_s starts with deformation equal to 2.02 mm and spring force equal to 2.40 6 N; these values increase along the upper plateau to become M_f; which has deformation equal to 19.8mm and spring force 6.007 N, respectively. At the lower plateau, the point transformation A_S has a deformation of 15.35 mm and a spring force equal to 2.194 N. These values decreased along the lower plateau to become the point transformation A_f, which has deformation equal to 3.03mm and spring force equal to -0.4839 N. The same behavior was also noticed for the stress- strain hysteresis loops because of the direct relationship between stress and force and the direct relationship between strain and deformation.

Stress increases with increasing force, and strain increases with increasing deformation in hysteresis loops. From Fig.8 (A and B), the transformation points of deformation and spring force increased with increasing ambient temperature because of the hysteresis loop shift, which indicates that nitinol earned thermal energy.

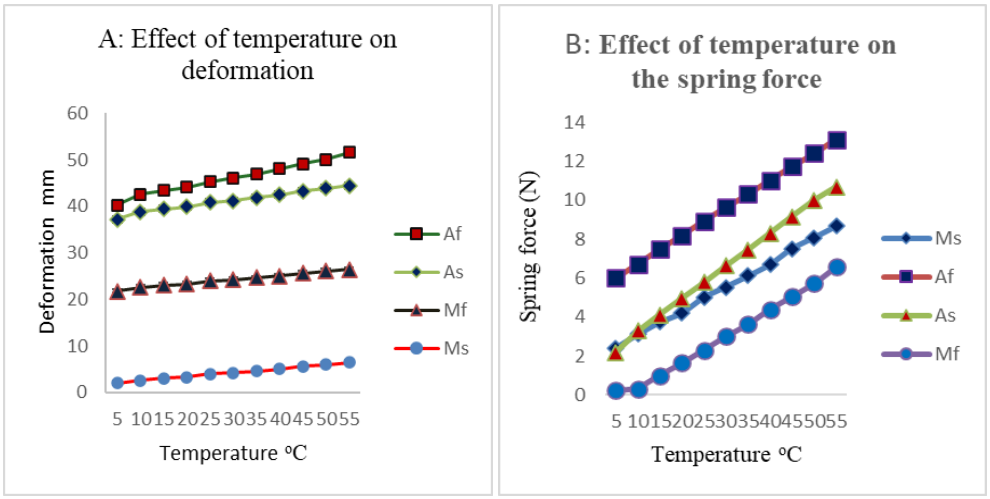

Figure 8: The effect of temperature on the points of transformation of (A) deformation, (B) spring force respectively.

4. Conclusions

The environmental temperature affects the hysteresis amount within the NiTi material. The width of the hysteresis loop indicates the effect of changing the environmental temperature on the material's energy gain. From (5 to 55) ^{o}C the hysteresis loop narrows with increasing temperature. This indicates that the amount of stress stored in the NiTi alloy during the austenite to martensite transformation will be less when the environmental temperature is higher. Also, the required stress that starts the reverse transformation is less at higher temperatures due to the thermal energy gained from the environment. The narrower hysteresis loop causes a lower shape memory effect. When changing the coil radius, the size of hysteresis loops did not change, but the transformation points changed with an increased coil radius. The size of the loop did not depend on the coil radius. This behavior for the Nitinol actuator shows that the actuator's efficiency increases with increasing temperature and spring height.

The deformation point increased with increasing temperature, while the spring force required for the transformation to start or finish decreased with increasing temperature because materials gained energy. The (M_s, M_f, A_s, and A_f) deformation points decrease with increasing wire radius. While the spring force points (M_s, M_f, A_s, and A_f) increase with increasing wire radius. The transformation point changes with increasing coil radius, while spring force points decrease with increasing coil radius. Deformation points (M_s, M_f, A_s, and A_f) change with increasing spring height. While spring force points (M_s, M_f, A_s, and A_f)) decrease with increasing spring height.

Conflict of interest

Authors declare that they have no conflict of interest.

References

1. M. N. Makdisi and Z. A. Al Shadidi, Iraqi J. Sci. **51**, 301 (2010).
2. C. Yu, H. M. Jiang, D. Song, Y. Zhu, and G. Kang, Int. J. Plastic. **165**, 103614 (2023).
3. S. Kadkhodaei and A. V. D. Walle, Acta Mat. **147**, 296 (2018).
4. G. Ren and H. Sehitoglu, Comput. Mat. Sci. **123**, 19 (2016).
5. X. Yang and J. Shang, Appl. Sci. **2021**, 6878 (2021).
6. D. Mulhall and M. J. Moelter, Am. J. Phys. **82**, 665 (2014).
7. X. Huang, C. Bungaro, V. Godlevsky, and K. M. Rabe, Phys.l Rev. B **65**, 014108 (2001).
8. J. M. S. Al-Murshdy and N. Y. Ali, in Journal of Physics: Conference Series, IOP Publishing, 2021, p. 012073.
9. S. B. Bakhtiar, PhD. Thesis, University of Western Australia, (2019).
10. S. A. Amin and A. Y. Hassan, J. Eng. Sustain. Dev. **23**, 1 (2019).
11. S. H. Ali, A. A. Eidan, and A. Al Sahlani, in IOP Conference Series: Materials Science and Engineering, IOP Publishing, 2021, p. 012009.
12. S. A. Mohammed, E. S. Kadhim, and R. M. Alwan, Iraqi J. Appl. Phys. **17**, 29 (2021).
13. G. Song, Smart Mat. Struc. **16**, 1796 (2007).
14. M. Kalmar, A. Boese, I. Maldonado, R. Landes, and M. Friebe, Med. Dev.: Evid. Res. **12**, 285 (2019).
15. L. C. Brinson, J. Intel. Mat. Syst. Struc. **4**, 229 (1993).
16. B. L. Franco, MSc. Thesis, Texas A and M University, (2014).
17. V. B. Krishnan, MSc. Thesis, University of Central Florida Orlando, (2004).
18. I. Chopra, AIAA J. **40**, 2145 (2002).

19. L. Petrini and F. Migliavacca, J. Metal. **2011**, 1 (2011).
20. J. Wang, B. Huang, X. Gu, J. Zhu, and W. Zhang, Int. J. Mech. Sci. **236**, 107744 (2022).
21. D. J. S. Ruth, Trans. Indian Nat. Acad. Eng. **6**, 523 (2021).
22. B. Koçkar, Shap. Mem. Superelast., (2023).
23. N. Farjam, R. Mehrabi, H. Karaca, R. Mirzaeifar, and M. Elahinia, in Behavior and Mechanics of Multifunctional Materials and Composites XII, SPIE, 2018, p. 187.
24. J. Meiser and H. M. Urbassek, Metals **8**, 837 (2018).
25. V. A. L'vov, E. Cesari, A. Kosogor, J. Torrens-Serra, V. Recarte, and J. I. Pérez-Landazábal, Metals **7**, 509 (2017).
26. B. Yuan, M. Zhu, and C. Y. Chung, Materials **11**, 1716 (2018).
27. S. Abbas, S. Maleksaeedi, E. Kolos, and A. J. Ruys, Materials **8**, 4344 (2015).
28. M. Petersmann, T. Antretter, G. Cailletaud, A. Sannikov, U. Ehlenbröker, and F.-D. Fischer, Int. J. Plast. **119**, 140 (2019).
29. A. Khudhair, F. Hatem, and D. Mohammed Ridha, Eng. Tech. J. **36**, 586 (2018).
30. C. Naresh, P. Bose, and C. Rao, in IOP conference series: materials science and engineering, IOP Publishing, 2016, p. 012054.
31. M. L. L. Júnior, L. Pino, M. Barati, L. Saint-Sulpice, L. Daniel, and S. A. Chirani, Smart Mat. Struc. **32**, 065002 (2023).
32. B. Dhakal, D. Nicholson, A. Saleeb, S. Padula, and R. Vaidyanathan, Smart Mat. Struc. **25**, 095056 (2016).
33. R. B. Sreesha, S. H. Ladakhan, D. Mudakavi, and S. M Adinarayanappa, Int. J. Adv. Manuf. Tech. **122**, 4421 (2022).
34. S. Singh, S. Karthick, and I. Palani, Vacuum **191**, 110369 (2021).
35. P. Shayanfard, L. Heller, P. Šandera, and P. Šittner, Eng. Fract. Mech. **244**, 107551 (2021).
36. J. G. Boyd and D. C. Lagoudas, Int. J. Plast. **12**, 805 (1996).
37. D. Lagoudas, D. Hartl, Y. Chemisky, L. Machado, and P. Popov, Int. J. Plast. **32**, 155 (2012).
38. W. Rączka, J. Konieczny, and M. Sibielak, Sol. St. Phenom. **199**, 365 (2013).
39. S. Enemark, I. F. Santos, and M. A. Savi, J. Intel. Mat. Sys. Struct. **27**, 2721 (2016).
40. A. Weirich and B. Kuhlenkötter, in Actuators, MDPI, 2019, p. 61.
41. Y. Zhang, C. Yu, Y. Zhu, Q. Kan, and G. Kang, Int. J. Mech. Sci. **236**, 107767 (2022).
42. H. De Souza Oliveira and A. S. De Paula, Smart Mat. Struct. **29**, 105033 (2020).
43. S. Mohan and A. Banerjee, Smart Mat. Struct. **30**, 055011 (2021).
44. S. S. Hiadrah, Iraqi J. Sci. **64**, 2843 (2023).
45. G. Cousland, X. Cui, A. Smith, A. Stampfl, and C. Stampfl, J. Phys. Chem. Sol. **122**, 51 (2018).
46. J. Schijve, *Fatigue of structures and materials*. 2nd Ed. (Dordrecht, Springer, 2009).
47. B. Yang, *Stress, Strain, and Structural Dynamics: An Interactive Handbook of Formulas, Solutions, and MATLAB Toolboxes*. (Burlington, USA, Academic Press, 2005).
48. D. Hartl, D. Lagoudas, F. Calkins, and J. Mabe, Smart Mat. Struct. **19**, 015020 (2009).
49. F. Auricchio, G. Scalet, and M. Urbano, J, Mat. Eng. Perform. **23**, 2420 (2014).
50. E. Toptas, M. F. Celebi, and S. Ersoy, J. Measur. Eng. **9**, 87 (2021).

تأثير أبعاد نابض NiTi والتأثير البيئي على خصائص المشغل

زينة عبد الامير الشديد[1]، احمد كاظم فالح[2] ، مهدي حسن سهيل[1] و سهى سالم حيدره[3]
[1]قسم تقنيات الأشعة و السونار، كلية المأمون الجامعة، بغداد، العراق
[2]قسم تقنيات الأشعة و السونار، الكلية الطبية التقنية، جامعة الفراهيدي، بغداد، العراق
[3]قسم الفيزياء، كلية التربية، جامعة ابين، ابين، اليمن

الخلاصة

يستخدم النيتينول في العديد من التطبيقات الطبية، بما في ذلك بدائل الأنسجة الصلبة ، بسبب خصائصه المناسبة، بما في ذلك معامل المرونة الوثيق لتلك الموجودة في العظام. للأهمية الكبيرة للخصائص الميكانيكية لهذه المادة في بدائل الأنسجة، تمت دراسة استجابة التباطؤ في محاولة لاستكشاف قدرة المادة على تذكر حالتها الميكانيكية السابقة بالإضافة إلى قدرتها على تحمل الإجهاد، للحصول على الأبعاد المناسبة لاستخدام نابض حلزوني النتنول كمشغل.يتم إجراء فحص الإجهاد والانفعال بطريقة حسابية باستخدام كود Lagoudas MATLAB عن طريق تغيير أنصاف أقطار الملف المختلفة ودرجات حرارة البيئة وأطوال الملف.

تم التحقيق في التباين في الخصائص الحرارية عن طريق تغيير درجة حرارة المحيط لمحرك نوابض NiTi الافتراضي. تمت دراسة حلقة التخلفية عن طريق زيادة الضغط الخارجي من أجل تحول مارتنسايت عكسي. يؤثر نصف قطر الملف وارتفاع الزنبرك ونصف قطر السلك على قوة الزنبرك والتشوهات. بنفس الطريقة، تؤثر هذه المعلمات على قيم الإجهاد والضغط. تظهر هذه التغييرات من خلال قيم البداية والنهاية Martensite و Austenite من بين هذه القيم، ميز الباحث أن أكثر المعلمات تأثراً هو نصف قطر السلك.

يعتمد حجم حلقة التخلفية في المشغل NiTi على درجة الحرارة المحيطة، وتضيق حلقة التباطؤ مع زيادة درجة الحرارة. عند درجة حرارة أعلى زادت القوة المزودة للمشغل وزاد التشوه؛ لذلك ، توفر درجة الحرارة المنخفضة عمرًا أطول للمشغل.

الكلمات المفتاحية: المرونة الفائقة، النتنول، مشغل، ماتلاب، حلقة الهسترة.